New members of the $[Ru(diimine)(CN)_4]^{2-}$ family: structural, electrochemical and photophysical properties

Harry Adams,[a] Wassim Z. Alsindi,[b] Graham M. Davies,[a] Martin B. Duriska,[a] Timothy L. Easun,[a] Hazel E. Fenton,[a] Juan-Manuel Herrera,[a] Michael W. George,*[b] Kate L. Ronayne,[c] Xue-Zhong Sun,[b] Michael Towrie[c] and Michael D. Ward*[a]

Received 27th June 2005, Accepted 5th September 2005
First published as an Advance Article on the web 14th September 2005
DOI: 10.1039/b509042c

A series of complexes of the type $K_2[Ru(\mathbf{NN})(CN)_4]$ has been prepared, in which **NN** is a diimine ligand, and were investigated for both their structural and photophysical properties. The ligands used (and the abbreviations for the resulting complexes) are 3-(2-pyridyl)pyrazole (**Ru-pypz**), 2,2′-bipyrimidine (**Ru-bpym**), 5,5′-dimethyl-2,2′-bipyridine (**Ru-dmb**), 1-ethyl-2-(2-pyridyl)benzimidazole (**Ru-pbe**), bidentate 2,2′:6′,2″-terpyridine (**Ru-tpy**). The known complexes with **NN** = 2,2′-bipyridine (**Ru-bpy**) and 1,10-phenathroline (**Ru-phen**) were also included in this work. A series of crystallographic studies showed that the $[Ru(\mathbf{NN})(CN)_4]^{2-}$ complex anions form a range of elaborate coordination networks when crystallised with either K^+ or Ln^{3+} cations. The K^+ salts are characterised by a combination of near-linear Ru–CN–K bridges, with the cyanides coordinating to K^+ in the usual 'end-on' mode, and unusual side-on π-type coordination of cyanide ligands to K^+ ions. With Ln^{3+} cations in contrast only Ru–CN–Ln near-linear bridges occurred, affording 1-dimensional helical or diamondoid chains, and 2-dimensional sheets constituted from linked metallamacrocyclic rings. All of the $K_2[Ru(\mathbf{NN})(CN)_4]$ complexes show a reversible Ru(II)/Ru(III) couple (*ca.* +0.9 V *vs.* Ag/AgCl in water), the exception being **Ru-tpy** whose oxidation is completely irreversible. Luminescence studies in water showed the presence of ^{3}MLCT-based emission in all cases apart from **Ru-bpym** with lifetimes of tens/hundreds of nanoseconds. Time-resolved infrared studies showed that in the ^{3}MLCT excited state the principal C–N stretching vibration shifts to positive energy by *ca.* 50 cm^{-1} as a consequence of the transient oxidation of the metal centre to Ru(III) and the reduction in back-bonding to the cyanide ligands; measurement of transient decay rates allowed measurements of ^{3}MLCT lifetimes for those complexes which could not be characterised by luminescence spectroscopy. A few complexes were also examined in different solvents (MeCN, dmf) and showed much weaker emission and shorter excited-state lifetimes in these solvents compared to water.

Introduction

The luminescent metal complex $[Ru(bpy)(CN)_4]^{2-}$,[1–3] introduced by Bignozzi and co-workers in 1986,[3] has received much less attention than $[Ru(bpy)_3]^{2+}$ as a component of polynuclear assemblies in the general field of supramolecular photochemistry, despite its many desirable properties. Like $[Ru(bpy)_3]^{2+}$ and related complexes,[4] it is luminescent from a relatively long-lived Ru → bpy ^{3}MLCT excited state, which is capable of effecting photoinduced energy- or electron-transfer to appropriate quenching molecules. There are however three significant properties of the $[Ru(bpy)(CN)_4]^{2-}$ unit which are of particular additional value but have been scarcely exploited.

Firstly, the strong solvatochromism of $[Ru(bpy)(CN)_4]^{2-}$, which arises from interaction of the externally-directed electron lone pairs on the cyanide ligands, means that its ^{3}MLCT energy and its ground and excited state redox potentials are highly solvent dependent; for example the ^{3}MLCT luminescence maximum varies from 640 nm in water to 818 nm in dmf, and the Ru(II)/Ru(III) redox potential varies from +0.77 V to −0.28 V (*vs.* ferrocene/ferrocenium) between the same solvents.[1] This also applies in the solid state: Mann and co-workers showed how a crystalline salt of $[Ru(bpy)(CN)_4]^{2-}$ could act as a humidity sensor because of its reversible colour change from purple to yellow in the presence of humidity, which is associated with water molecules forming hydrogen-bonds to the externally-directed lone pairs of the cyanide ligands.[5] We[6] and others[7] have exploited this effect by using changes in solvent to alter the ability of $[Ru(bpy)(CN)_4]^{2-}$ to act as an energy-donor in simple dyad molecules: changing the solvent alters the energy available to the $[Ru(bpy)(CN)_4]^{2-}$ energy-donor unit without significantly affecting the receiving energy level on the acceptor component, so the gradient for photoinduced energy-transfer can be finely controlled.

Secondly, the cyanide ligands can act as bridging ligands to additional metal ions, allowing formation of Ru–CN–M bridged coordination oligomers and polymers by simple combination of $[Ru(bpy)(CN)_4]^{2-}$ with other metal cations. We have recently described coordination polymers based on combination of

[a]*Department of Chemistry, University of Sheffield, Sheffield, UK S3 7HF. E-mail: m.d.ward@Sheffield.ac.uk*
[b]*School of Chemistry, University of Nottingham, University Park, Nottingham, UK NG7 2RD. E-mail: mike.george@Nottingham.ac.uk*
[c]*CCLRC Rutherford Appleton Laboratory, Chilton, Didcot, Oxon, UK OX11 0QX*

$[Ru(bpy)(CN)_4]^{2-}$ with lanthanide(3+) salts[8,9] in which excitation of the Ru-based MLCT transition results in energy-transfer to, and sensitised luminescence from, lanthanide cations such as Yb(III), Nd(III), Er(III) and Pr(III) which have low-lying emissive levels and display sensitised near-infrared luminescence.[9] Scandola and co-workers described a while ago energy-transfer between $[Ru(bpy)_2(CN)_2]$ and a Cr(III)-macrocycle unit which were connected by Ru–CN–Cr bridges in a similar way.[10]

Thirdly, the IR-active cyanide ligands of $[Ru(bpy)(CN)_4]^{2-}$ allow the movement of excitation energy and electrons in polynuclear complexes to be monitored by transient IR spectroscopy, since the CN vibrations are sensitive to redistribution of electron density in the complex; this technique is well known for carbonyl ligands in complexes such as $[Re(bpy)(CO)_3Cl]$ and its derivatives,[11] but has been applied to luminescent cyanometallate complexes in very few cases.[12]

Despite these advantages, analogues and derivatives of $[Ru(bpy)(CN)_4]^{2-}$ have been scarcely studied, beyond simple replacement of bpy by phenanthroline or addition of methyl substituents.[13] This is in marked contrast to the vast number of analogues of $[Ru(bpy)_3]^{2+}$ that have been investigated in the last few decades.[4] As part of a program of research into the photophysical properties of complexes of this type we have prepared a series of analogues in which the bpy ligand is replaced by other diimines. In the course of this work we have found that these $[Ru(\mathbf{NN})(CN)_4]^{2-}$ complexes (**NN** is a diimine ligand) form a varied and attractive series of coordination networks with s- and f-block metal counter-ions, and the structural chemistry of these complexes is of as much interest as their photophysics. Heterometallic coordination networks based on cyanometallates have of course been of enduring interest for many years. In many cases the cyanometallate anion on which the network is based is an octahedral hexacyanometallate;[14] however cyanometallates with different structures such as octadentate $[W(CN)_8]^{3-/4-}$,[15] C_{2v}-symmetric tetradentate $[Fe(bpy)(CN)_4]^-$ and $[Fe(phen)(CN)_4]^-$,[16] square planar $[M(CN)_4]^{2-}$ (M = Ni, Pd),[17] and linear bidentate $[M(CN)_2]^-$ (M = Ag, Au)[18] have also been used recently as the basis of 1-, 2- or 3-dimensional networks based on cyanide bridges spanning two different metal ions.

This paper, therefore, describes the syntheses and structural characterisation of several coordination networks based on $[Ru(\mathbf{NN})(CN)_4]^{2-}$ species with either potassium or lanthanide cations. We note that structural studies on $[Ru(bpy)(CN)_4]^{2-}$ and its relatives are almost unknown, with the only examples currently on the Cambridge Structural Database being those referred to above.[5,8,9] In addition, this paper describes the solution spectroscopic, redox and photophysical properties of the new $[Ru(\mathbf{NN})(CN)_4]^{2-}$ species, including time-resolved IR studies of the ^{3}MLCT states of some members of the series.

Results and discussion

Syntheses of new diimine–tetracyanoruthenate complexes

The new complexes prepared, together with their abbreviations, are listed in Scheme 1. All were prepared in the same basic way, by reaction of the diimine ligand with potassium hexacyanoruthenate in an aqueous acidic medium followed by ion-exchange chromatography to give the complexes as their dipotassium salts.

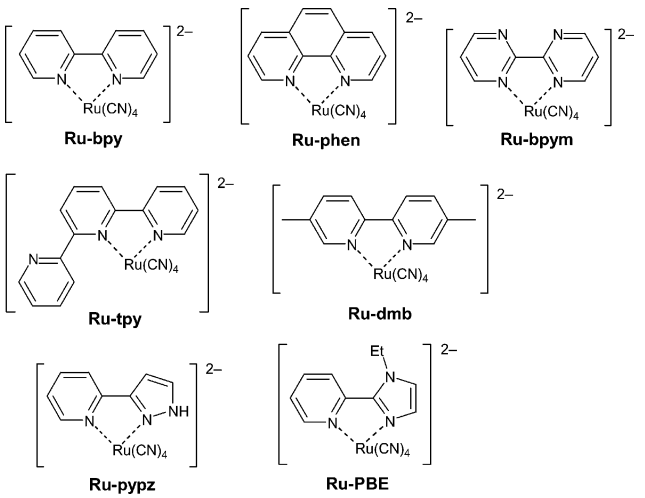

Scheme 1

All complexes were characterised by ^{1}H NMR spectroscopy and negative-ion electrospray mass spectrometry; elemental analyses always indicated the presence of several water molecules, as subsequently borne out by the crystallographic studies. Routine characterisation data are summarised in the Experimental section.

Of the complexes, **Ru-bpy** and **Ru-phen** are already known.[1,13] **Ru-pypz**, **Ru-dmb** and **Ru-PBE** are simple analogues of $[Ru(bpy)(CN)_4]^{2-}$ but based on different diimine ligands available from the literature.[19,20] **Ru-bpym** was prepared to see how the presence of a vacant bipyrimidine-based coordination site, in addition to the cyanide-based coordination sites, would alter the structural properties. **Ru-terpy** was the unexpected result of an attempt to prepare $[Ru(terpy)(CN)_3]^-$, a known compound[21] but whose synthesis requires the use of potassium cyanide. We were interested to see if a more user-friendly synthesis could be achieved from hexacyanoruthenate and terpyridine; however this yielded **Ru-terpy** in which the NMR spectrum clearly showed that the terpyridine was asymmetrically coordinated as a bidentate ligand, with all 11 protons inequivalent—something which terpyridine is known to do in other complexes.[22] Under the conditions of the reaction we found no evidence for formation of $[Ru(terpy)(CN)_3]^-$ by this route.

Structures of potassium salts

The complex $K_2[Ru(phen)(CN)_4]$ is known[13] but has not previously been structurally characterised; the structure of $K_2[Ru(phen)(CN)_4]\cdot 4H_2O$ turns out to show some interesting features. The complex anion itself has an unremarkable pseudo-octahedral geometry, as it does an all of the structures reported in this paper, with typical Ru–N and Ru–C bond distances. Each of the potassium cations is coordinated in a side-on manner by a pair of *cis*-related cyanide ligands from the $[Ru(phen)(CN)_4]^{2-}$ unit (Fig. 1); the K–N and K–C separations in this interaction average 3.01 and 3.08 Å respectively, with C–K–N angles being 21.9° (Fig. 1). This type of interaction between cyanides and alkali metal ions has recently been observed by Rauchfuss *et al.* in numerous cyanometallate cages, where bridging cyanides along the edges of a cage are also interacting in a side-on manner with an alkali metal cation trapped in the centre of the cavity, and is presumably a weak electrostatic interaction.[23] Gokel has demonstrated similar side-on interactions

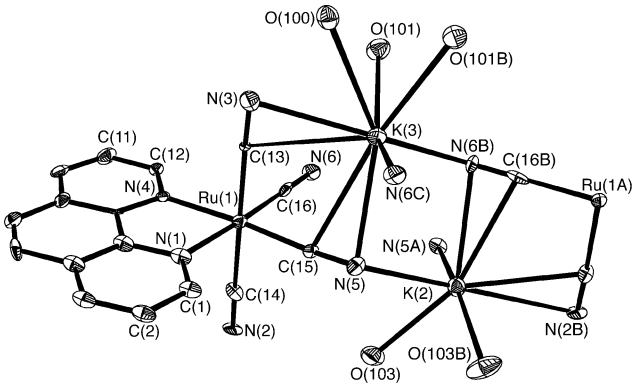

Fig. 1 ORTEP diagram of the asymmetric unit of $K_2[Ru(phen)(CN)_4]\cdot 4H_2O$, with some additional symmetry-equivalent atoms included to complete the coordination spheres around the metal atoms.

between alkene/alkyne units and alkali metal cations,[24] and we recently observed it in complexes of $[Ru(bpy)(CN)_4]^{2-}$ such as $[\{Ru(bpy)(CN)_4\}_2\{Ln(H_2O)_m\}\{K(H_2O)_n\}]\cdot xH_2O$ (Ln = Pr, Er, Yb).[8] In $K_2[Ru(phen)(CN)_4]$ the K–C and K–N separations are comparable to those observed in the few other examples of K^+ cyanide[23]/alkyne[24] complexes of this type. The K^+ ions are also coordinated by two [K(2)] or three [K(3)] water molecules, as well as the N atoms from two 'end-on' cyanides. Thus, K(2) is coordinated by two side-on cyanides, two water molecules, and two additional cyanide ligands *via* the N atoms only; K(3) is similar but with an additional water molecule. It is notable that two of the cyanide ligands (the ones in the same plane as the phenanthroline ligand) have an extensively bridging coordination mode, being C-bound to the Ru atom, CN side-on bound to a K^+ ion, and having the N-terminal lone pair shared between an additional two K^+ ions. This bridging behaviour of the cyanide ligands, as well as bridging of K^+ ions by water molecules [O(101) and O(103)], results in formation of a one-dimensional polymeric chain which propagates along the crystallographic *c* axis (Fig. 2).

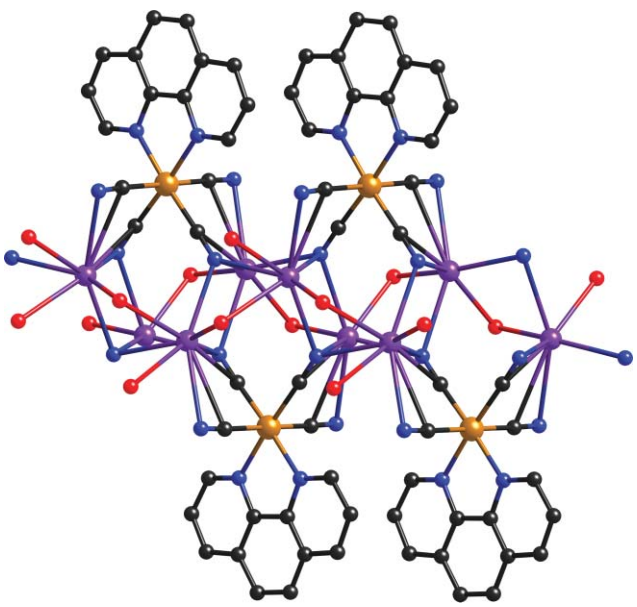

Fig. 2 View of the coordination chain in $K_2[Ru(phen)(CN)_4]\cdot 4H_2O$ (Ru = brown; K = purple; N = blue, O = red, C = black).

$K_2[Ru(bpym)(CN)_4]\cdot 3H_2O$ has an entirely different structure. The $[Ru(bpym)(CN)_4]^{2-}$ complex anion has a K^+ cation occupying the second NN-chelating site of the bipyrimidine ligand. This atom [K(2)] is further coordinated by three water molecules, all of which are involved in bridging interactions to other K^+ ions, and the N atoms of two cyanide ligands from separate $[Ru(bpym)(CN)_4]^{2-}$ complex anions (Fig. 3). The coordination geometry about K(2) is approximately pentagonal bipyramidal, with N(8C) and O(3) being the axial ligands [N–K–O angle, 172.7°] and the sum of the five angles in the plane being 360.2°. K(1) in contrast is coordinated in a side-on manner by five cyanide ligands from two different $[Ru(bpym)(CN)_4]^{2-}$ complex anions, in addition to three water molecules (which are all involved in bridging to another K^+ ion). These interactions are slightly longer than in the structure of $K_2[Ru(phen)(CN)_4]$, with the K–N and K–C side-on interactions averaging 3.22 and 3.25 Å respectively; the coordination environment of K(1) is included in Fig. 3. The combination of multiply bridging cyanide ligands, as well as bridging water ligands between K^+ ions, results in propagation of the structure into a three-dimensional network. This consists of 2-D sheets, as shown in Fig. 4, which are connected in the third dimension by water ligands [O(1)] which cross-link the sheets by connecting K(1) in one sheet with K(2) in the next. In addition, the bipyrimidine ligands of sheets interpenetrate such that there is an alternating π-stacking interaction between them. It is noticeable from Fig. 4 how some of the cyanide ligands can interact with four different metal ions, being C-bound to the ruthenium centre,

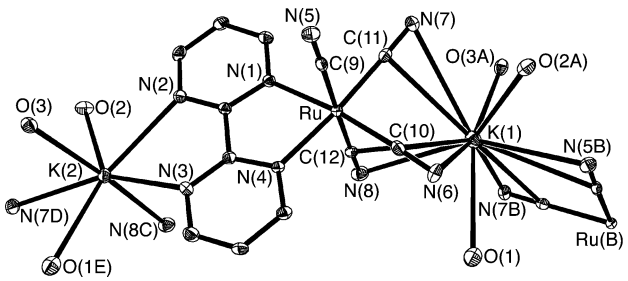

Fig. 3 ORTEP diagram of the asymmetric unit of $K_2[Ru(bpym)(CN)_4]\cdot 3H_2O$, with some additional symmetry-equivalent atoms included to complete the coordination spheres around the metal atoms.

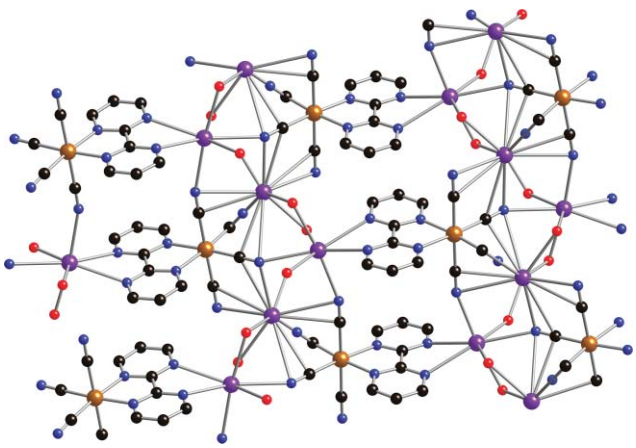

Fig. 4 View of the two-dimensional sheet structure of $K_2[Ru(bpym)(CN)_4]\cdot 3H_2O$ (Ru = brown;, K = purple; N = blue, O = red, C = black).

involved in side-on binding with two different K^+ ions, and also acting as a terminal N-donor ligand to a third K^+ centre.

The structure of $K_2[Ru(\kappa^2\text{-terpy})(CN)_4]\cdot MeOH\cdot 0.5H_2O$, in which the terpy ligand is bidentate, is likewise dominated by side-on cyanide $\cdots K^+$ interactions (Fig. 5, 6). K(2) is coordinated in this manner by two cyanide ligands from each of two $\{Ru(CN)_4\}^{2-}$ units, with average $K\cdots C$ and $K\cdots N$ distances of 3.18 and 2.96 Å respectively; it also has one coordinated methanol ligand and a pyridyl ligand, which is the pendant 2-pyridyl group from a terpyridine whose other two donors are coordinated to ruthenium. K(1) in contrast is coordinated by two O atoms from (bridging) methanol ligands and the N atoms from three end-on cyanide ligands (Fig. 5). The combination of the bridging interactions involving cyanide and methanol ligands results in formation of a two-dimensional network. This is made up from 1-D chains which are based on alternating $[Ru(terpy)(CN)_4]^{2-}$ and K(2) units, which are disposed such that the $Ru\cdots K\cdots Ru\cdots K$ sequence forms a zig-zag chain (Fig. 6) which is held together principally by the side-on cyanide $\cdots$ K(2) bonding interactions. These chains are linked side-by-side to make a two-dimensional sheet by the K(1) centres which interact with the externally-directed O and N(cyanide) donors, as shown in Fig. 5. As with the other two structures of potassium salts, the cyanide bridges are both simultaneously side-on coordinated and terminally coordinated to different K^+ ions.

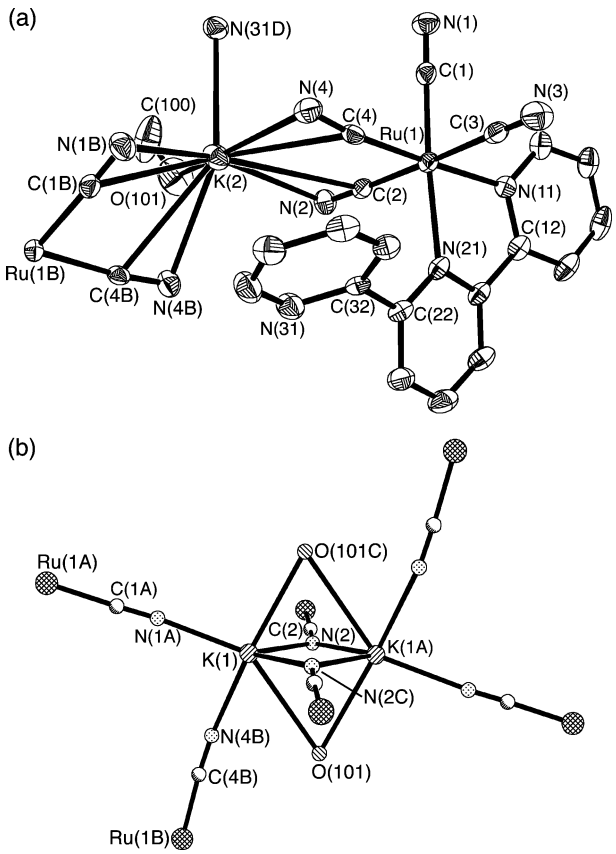

Fig. 5 (a) ORTEP diagram of part of the asymmetric unit of $K_2[Ru(\kappa^2\text{-terpy})(CN)_4]\cdot MeOH\cdot 0.5H_2O$, emphasising the interaction of the cyanoruthenate anions with K(2) *via* side-on π-type cyanide coordination to K(2); (b) diagram of the coordination environment around K(1).

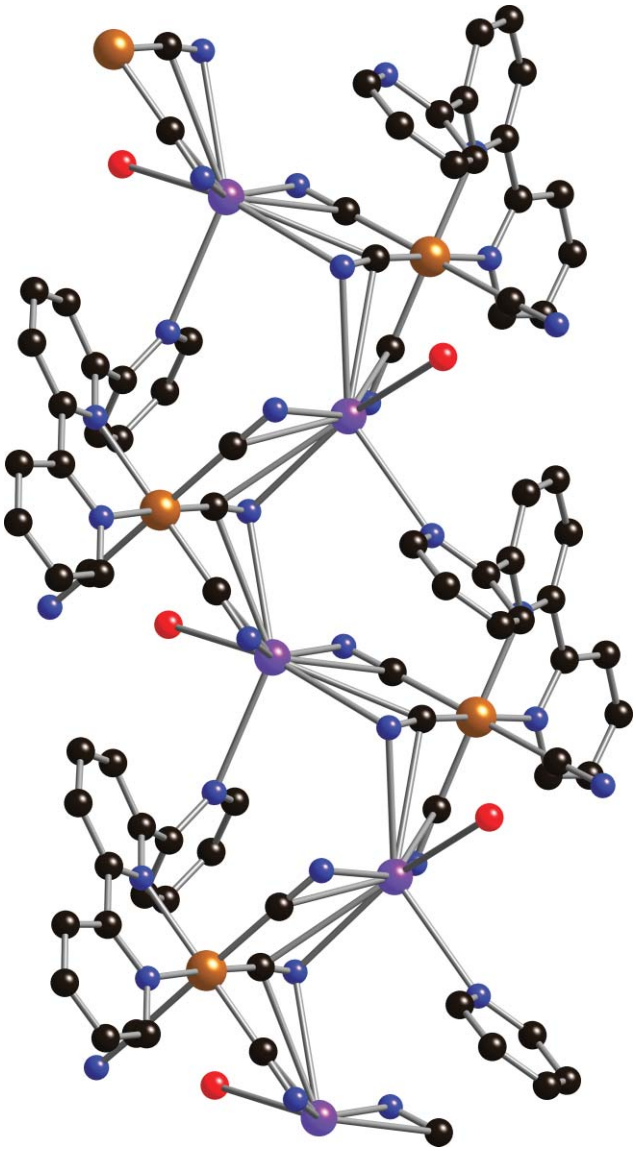

Fig. 6 View of the one-dimensional coordination network $K_2[Ru(\kappa^2\text{-terpy})(CN)_4]\cdot MeOH\cdot 0.5H_2O$ formed by interaction of the cyanoruthenate anion with K(2); these chains are connected side-by-side by bridging cyanide interactions with K(1) (as in Fig. 5a) (Ru = brown; K = purple; N = blue, O = red, C = black).

Structures of lanthanide salts

Slow evaporation of aqueous solutions containing the potassium salts of the $[Ru(diimine)(CN)_4]^{2-}$ units and a lanthnide nitrate afforded, in some cases, new coordination networks based on Ru–CN–Ln bridges, of which three have been structurally characterised.

The crystal structure of $KEr[Ru(PBE)(CN)_4]_2\cdot 10H_2O$ (Fig. 7, 8) shows a combination of the side-on cyanide $\cdots K^+$ interactions seen in the earlier structures, as well as terminal Ru–CN–Er bridges. The structure is a one-dimensional chain consisting of $Ru_2Er_2(\mu\text{-}CN)_4$ diamonds in which the Er centres are shared between successive diamonds (Fig. 7). Each Er(III) centre is 8-coordinate, from four cyanide N atoms and four water ligands. The situation is more complex than is apparent from Fig. 7 because

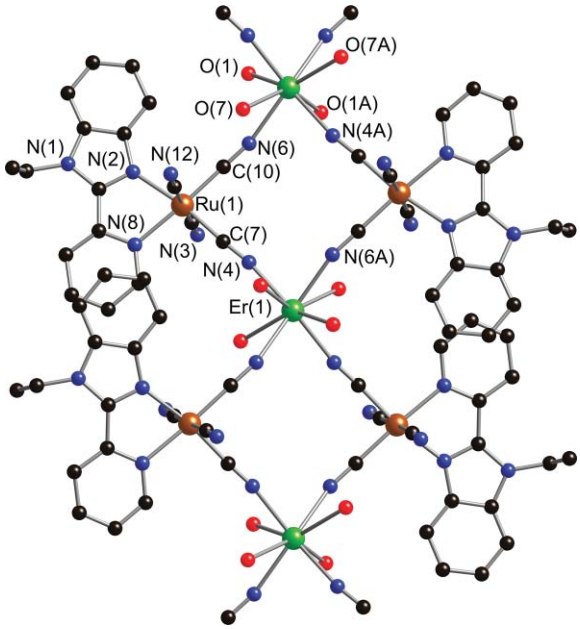

Fig. 7 View of the one-dimensional diamondoid chain of KEr[Ru(PBE)$(CN)_4]_2\cdot 10H_2O$, with potassium atoms omitted for clarity (Ru = brown, Er = green; N = blue, O = red, C = black).

two of the water ligands [O(3), O(7)] are disordered over two sites with 50% occupancy in each; only one component of the disorder is shown in the figure. The Er–N and Er–O distances average 2.37 and 2.42 Å respectively, and the Ru $\cdots$ Er separations across the cyanide bridges are 5.417 and 5.498 Å. Given the disorder in the coordination sphere of Er(1) a description of its coordination geometry is inappropriate. The propensity of the K^+ ions to become involved in side-on interactions with cyanide ligands is demonstrated by the environment of K(1) (Fig. 8). These ions are located above and below the $Ru_2Er_2(\mu\text{-}CN)_4$ diamonds, with 50% occupancy in each site, such that they interact approximately equally with all four cyanide ligands in the diamond; the average K–C and K–N distances are 3.22 and 3.10 Å. Each K^+ ion also has a terminal water ligand [O(4); K(1)–O(4), 2.39 Å] and two additional water molecules [O(3) and O(7); 50% site occupancy each; K–O separations 2.90 Å] which are bridging to Er(1).

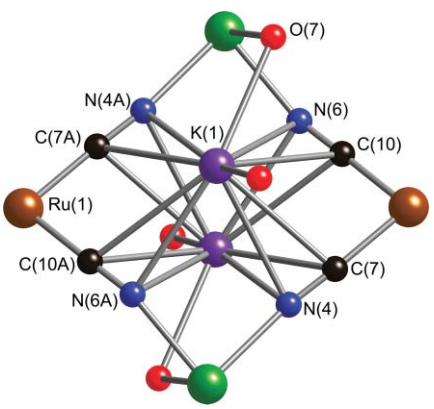

Fig. 8 A view of part of the structure of KEr[Ru(PBE)$(CN)_4]_2\cdot 10H_2O$ illustrating the disorder of the potassium atom and its associated water ligands (Ru = brown, Er = green; K = purple; N = blue, O = red, C = black).

The structure of $KEu[Ru(pypz)(CN)_4]_2\cdot 10.5H_2O$ (Fig. 9, 10) is quite different from this [and from the earlier-described complexes of $[Ru(bpy)(CN)_4]^{2-}$ with lanthanide cations].[8] It is a remarkably elaborate structure whose two main structural motifs are shown in Fig. 9 and 10. The tetracyanoruthenate anions and Eu(III)

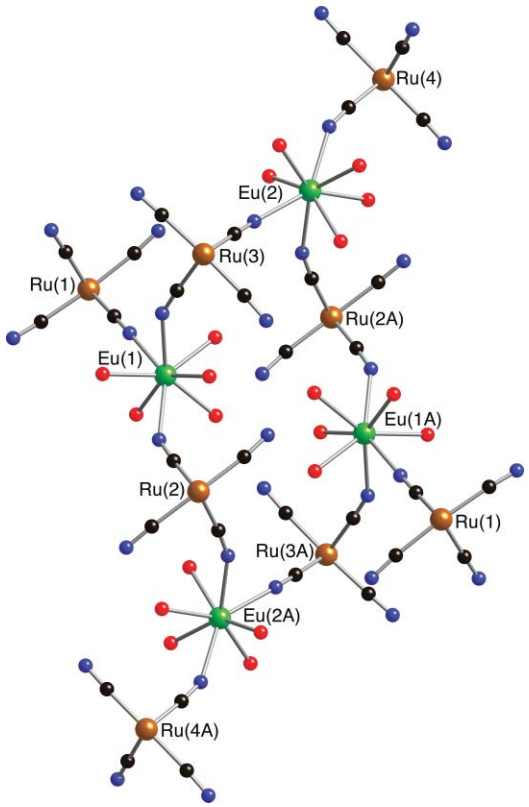

Fig. 9 A view of the large metallamacrocyclic ring in KEu[Ru(pypz)$(CN)_4]\cdot 10.5H_2O$, showing only the Ru and Eu atoms and the bridging cyanide ligands and the terminal water ligands (Ru = brown, Eu = green; N = blue, O = red, C = black).

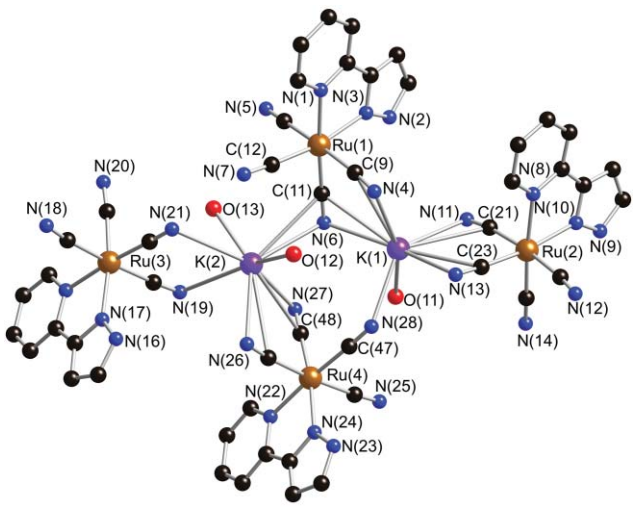

Fig. 10 A view of part of the lattice of $KEu[Ru(pypz)(CN)]\cdot 10.5H_2O$ showing how four cyanoruthenate units which are 'spokes' from the Ru_4Eu_4 rings (see Fig. 9) are connected by a combination of end-on and side-on cyanide coordination to K^+ ions (Ru = brown, Eu = green; K = purple; N = blue, O = red, C = black).

cations form a 24-membered ring based on four of each unit linked in a $\{Ru–CN–Eu–NC–\}_4$ cyclic sequence. Pendant from each Eu vertex is an additional $[Ru(pypz)(CN)_4]^{2-}$ unit which is connected to the Eu(III) by a single cyanide bridge. Accordingly, the $[Ru(pypz)(CN)_4]^{2-}$ units in the ring [based on Ru(2) and Ru(3)] have two cyanides involved in bridging interactions to adjacent Eu(III) sites, whereas the 'exocyclic' $[Ru(pypz)(CN)_4]^{2-}$ units [based on Ru(1) and Ru(4)] have only one cyanide involved in bridging to Eu(III). Each Eu(III) centre is accordingly eight-coordinate, from three bridging cyanides (two within the macro-ring and one from outside it) and five water ligands. The Ru···Eu separations across the cyanide bridges are in the range 5.32–5.58 Å. These rings are associated by cyanide bridging interactions to the K^+ ions, as shown in Fig. 10, which illustrates how four $[Ru(pypz)(CN)_4]^{2-}$ units, each from a different Ru–Eu ring, are associated by a combination of end-on Ru–CN–K^+ and side-on cyanide/K^+ interactions. K(1) is coordinated by four cyanides in a side-on manner, as well as one end-on cyanide [N(28)] and one water molecule [O(11)]. K(2) has three side-on cyanides, two of which are 'end-on' (although the C–N–K angles are far from linear) and two water molecules.

In complete contrast, the structure of $[Eu(NO_3)(H_2O)_5][Ru(bpym)(CN)_4]$ is a relatively simple one-dimensional helical chain (Fig. 11, 12). In this case there is a 1 : 1 ratio of Eu(III) and $[Ru(bpym)(CN)_4]^{2-}$ centres, with charge balance being provided by a nitrate ion attached to Eu(III). The Eu(III) centres are 9-coordinate from five water ligands, a bidentate nitrate [although one Eu–O bond from the nitrate is considerably longer than the other: Eu(2)–O(5), 2.477 Å; Eu(2)–O(6), 2.774 Å] and two N-donor cyanide ligands, each from a separate $[Ru(bpym)(CN)_4]^{2-}$ unit. The inset to Fig. 12 shows how the ···Ru–CN–Eu–NC–Ru··· sequence forms a spiral, with a pitch of 12.45 Å. The space group is chiral ($Pna2_1$) so this complex has spontaneously resolved on crystallisation to give optically pure individual crystals.

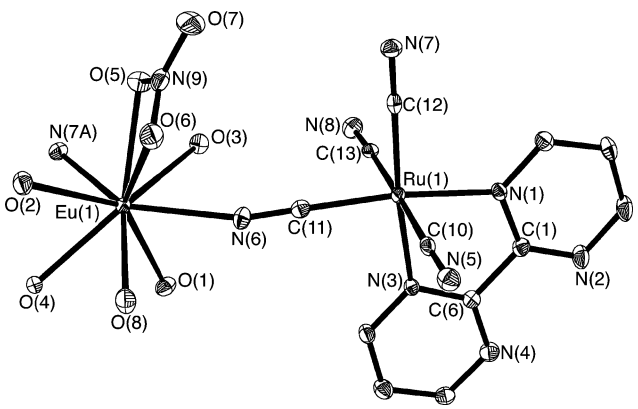

Fig. 11 ORTEP diagram of the asymmetric unit of $[Eu(NO_3)(H_2O)_5][Ru(bpym)(CN)_4]$, with some additional symmetry-equivalent atoms included to complete the coordination spheres around the metal atoms.

Electrochemistry

Cyclic voltammetric studies of the potassium salts of the cyanoruthenate complexes in water showed that all but one of the complexes show a reversible, one-electron process. By analogy

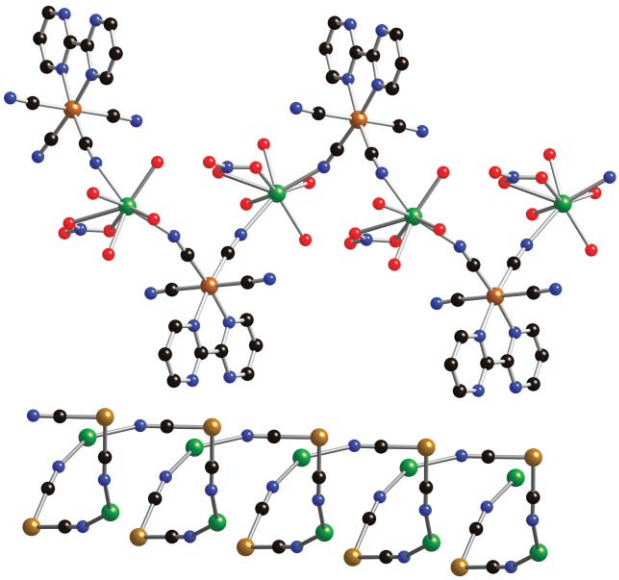

Fig. 12 Two views of $[Eu(NO_3)(H_2O)_5][Ru(bpym)(CN)_4]$ illustrating formation of a one-dimensional helical coordination polymer; the top view shows all atoms, whereas the lower shows only Ru, Eu and the bridging cyanide ligands (Ru = brown, Eu = green; N = blue, O = red, C = black).

with the known behaviour of $[Ru(bpy)(CN)_4]^{2-}$,[1] we assign this as a metal-centred Ru(II)/Ru(III) couple; with our experimental setup the Ru(II)/Ru(III) couple of $[Ru(bpy)(CN)_4]^{2-}$ occurs at +0.89 V *vs.* Ag/AgCl, close to the values for the new complexes. The redox potentials are listed in Table 1. In most cases the process is reversible (peak–peak separation 60–80 mV, equal cathodic and anodic peak currents, peak current proportional to square root of scan rate) on the voltammetric timescale. For **Ru-tpy** however the process is completely irreversible with no return wave. A possible explanation for this is that following oxidation the pendant pyridyl group displaces a cyanide ligand and becomes coordinated to the metal centre; there is no other apparent reason why this alone of all the complexes should show irreversible behaviour on oxidation. The strong π-accepting effects of 2,2′-bipyrimidine are apparent, with the Ru(II)/Ru(III) redox potential being at a more positive potential (+1.05 V *vs.* Ag/AgCl) than all the others (+0.7 to +0.89 V) because the metal centre is more electron-deficient.

The expected ligand-centred reductions were not accessible within the limits of the potential window provided by water as solvent.

Absorption and luminescence properties

In aqueous solution all of the complexes (as their potassium salts) display a band attributed to a Ru → diimine MLCT transition in the region around 400 nm (Table 1). For **Ru-bpym**, uniquely in the series, there are two clearly-resolved transitions in water, at 342 and 438 nm. In two cases the complexes were also slightly soluble in MeCN, and in these cases comparison with the spectra recorded in water shows the strong solvatochromic behaviour,[1] with the ^{1}MLCT absorption resolved into two components of which one moves to much lower energy. Thus, for example, in **Ru-dmb** the MLCT absorption maximum in water occurs at 393 nm, whereas in MeCN there are two clearly-resolved transitions at 372 and

Table 1 UV/Vis spectroscopic and photophysical data for the new complexes, measured in D_2O except where stated otherwise

Complex	UV/Vis absorptions λ_{max}/nm ($10^{-3}\varepsilon$/M^{-1} cm^{-1})	λ_{em}/nm	τ/ns	Φ	E^d/V
Ru-dmb	261 (9.6), 291 (15), 393 (2.1) [372, 514][a]	621 [758][a]	370 [36][a]	0.03 [0.002][a]	+0.85
Ru-tpy	296 (22), 411 (2.7)	647	106	0.025	+0.70[e]
Ru-bpym	342 (5.8), 437 (2.2) [415, 575][a]	—	3.4[b] [0.25][a,b]	—	+1.05[f]
Ru-PBE	242 (15), 313 (17), 404 (3.6)	665	471 [4.5][c]	0.007	+0.79
Ru-pypz	229 (23), 272 (20), 353 (6.9)	554	17	0.001	+0.83

[a] Figures in square brackets refer to measurements made in MeCN; extinction coefficients of absorption spectra not measured due to poor solubility. [b] Lifetime determined from transient IR spectra rather than luminescence as luminescence in solution was very weak. [c] Figures in square brackets refer to measurements made in dmf from transient IR spectra. [d] Redox potential for Ru(II)/Ru(III) couple in water/0.1 M KCl. For comparison the known complexes $[Ru(bpy)(CN)_4]^{2-}$ and $[Ru(phen)(CN)_4]^{2-}$ have redox potentials (measured with the same experimental setup) of +0.89 and +0.88 V *vs.* Ag/AgCl. [e] Irreversible (no return wave); the quoted potential is the peak potential on the outward sweep. [f] Reversibility difficult to judge as this process is very close to the rapidly-rising background associated with the solvent cutoff.

514 nm. For **Ru-bpym** the two transitions apparent in water (342, 437 nm) are both red-shifted to 415 and 575 nm respectively in MeCN.

In every case, in D_2O solution, excitation into the ^{1}MLCT absorption results in luminescence in the range 550–670 nm which is believed to originate from the ^{3}MLCT excited state. Kovács and Horváth recently showed that using D_2O as solvent afforded considerably longer-lived luminescence from complexes of this type than H_2O due to attenuation of non-radiative decay pathways in D_2O, a consequence of hydrogen-bond formation with the cyanide lone pairs.[13] In addition to examining all of the new complexes, for comparison purposes we also re-measured the properties of **Ru-bpy** and **Ru-phen** and found a satisfactory agreement between our measurements and those published previously.[1,13] A few effects are worth pointing out.

Firstly, for **Ru-tpy** the ^{1}MLCT absorption and ^{3}MLCT luminescence are red-shifted compared to **Ru-bpy**, despite the donor set being nominally identical. This we ascribe to the long bond Ru(1)–N(8) [2.190(5) Å], involving the central ring of the terpyridyl ligand, which is lengthened by virtue of having a sterically bulky group—the pendant pyridyl residue—at its C^2 position, *ortho* to the site of coordination. Lengthening this bond will weaken the ligand field of the coordinated bipyridyl fragment compared to normal un-encumbered bpy (Ru–N separation *ca.* 2.10 Å), which will slightly raise the d(π) orbital set and hence reduce the MLCT absorption and emission energies. This phenomenon has been observed in derivatives of $[Ru(bpy)_3]^{2+}$ in which the bpy ligands have a bulky substituent at the C^2/C^6 position.[25]

Secondly, variation in the nature of the diimine ligand results in significant changes to the ^{1}MLCT absorption and ^{3}MLCT luminescence energies for electronic reasons. The highest-energy absorption and luminescence in the series come from **Ru-pypz** (luminescence in water at 554 nm), implying that the pypz ligand has a higher-energy LUMO than the other diimines. [The alternative possible explanation, that the d(π) orbitals are lower in energy than in the other complexes, is not borne out by the electrochemical studies, as the Ru(II)/Ru(III) couple is not at an unusually positive potential compared to the other complexes]. This is also borne out by the short luminescence lifetime (17 ns) which is a consequence of the high-lying ^{3}MLCT state being close in energy to the metal-centred d–d state, which would provide a facile thermally-activated route for radiationless deactivation. Despite the relatively short luminescence lifetime, the high ^{3}MLCT energy of **Ru-pypz** will make it of particular value as an energy-donor in polynuclear assemblies.[26]

Thirdly, the luminescence of **Ru-bpym** is too weak to allow the excited-state lifetime to be measured by luminescence methods. Replacement of bpy by bipyrimidine has been shown in other complexes to result in much weaker, shorter-lived emission: for example $[Re(bpy)(CO)_3Cl]$ has $\lambda_{em} = 642$ nm, $\tau = 39$ ns and $\phi = 3 \times 10^{-3}$ (2-methyl-thf, fluid solution)[27] whereas $[Re(bpym)(CO)_3Cl]$ has $\lambda_{em} = 689$ nm, $\tau = 2.1$ ns and $\phi = 10^{-4}$ (CH_2Cl_2, fluid solution).[28] A similar effect is seen when bpy is replaced by bipyrimidine in Pt-diimine-diacetylides $[Pt(\mathbf{NN})(CCR)_2]$,[28,29] and is a consequence of the energy-gap law; the lower energy of the ^{3}MLCT excited state of **Ru-bpym**, arising from the lower energy of the bpym π* orbitals compared to bpy, means that the excited state is more efficiently quenched by molecular vibrations.

Finally, we note that for **Ru-dmb**, which is slightly soluble in MeCN, the emission maximum (like the lowest-energy MLCT absorption maximum) is substantially red-shifted compared to the situation in water, from 621 to 758 nm, and is much weaker—actually barely detectable—and short lived (see Table 1), in keeping with expectations based on the known solvatochromic behaviour of complexes of this type.[1]

Time-resolved infrared studies

All of these complexes should theoretically have four IR-active CN vibrations. In the solid state these are apparent as three closely-spaced strong peaks between about 2030 and 2060 cm^{-1} (sometimes not all three components are resolved), and a weaker peak at around 2090 cm^{-1} (see Table 2).

In aqueous solution these are not all resolved; the three closely-spaced peaks merge to give a strong peak at 2050–2060 cm^{-1}, and a weaker one appearing as a shoulder about 20–30 cm^{-1} higher. Fig. 13 shows the time-resolved difference IR spectrum of **Ru-bpym** obtained 100 ps after 400 nm excitation into the ^{1}MLCT absorption band. The parent ν(CN) vibrations are bleached, and weaker new bands appear at higher energy. Assuming that the most intense new transient corresponds to the most intense peak in the ground-state spectrum, there is a shift to higher energy of 52 cm^{-1} of this ν(CN) vibration when the complex is in the ^{3}MLCT excited state, as a consequence of loss of electron density on the Ru centre [which is transiently oxidised to Ru(III)] and the concomitant decrease in Ru(dπ) → CN(π*) back-bonding. The

Table 2 Infrared spectroscopic data in the ground and excited states

Complex	ν_{CN} (ground state)[a]/cm^{-1}	Main bleach in TRIR[b]/cm^{-1}	Main new transient in TRIR[b]/cm^{-1}	Δ/cm^{-1}
Ru-bpy	2032(s), 2047(s), 2056(s), 2089(m)	2051	2103	52
Ru-dmb	2034(s), 2040(s), 2054(s), 2090(m)	2049 [2068][c]	2095 [2104][c]	46 [36][c]
Ru-phen	2032(s), 2038(s), 2047(s), 2088(m)	2051	2098	47
Ru-tpy	2041(s), 2047(s), 2091(m)	2051	2100	49
Ru-bpym	2046(s), 2057(s), 2065(s), 2102(m)	2057 [2068][c]	2105 [2098][c]	48 [30][c]
Ru-PBE	2028(s), 2044(s), 2085(m)	2048	2095	47
Ru-pypz	2028(s), 2045(s), 2052(s), 2092(m)	2050	2098	48

[a] Solid-state spectra measured on powdered sample using diamond-ATR cell. [b] Figures in square brackets refer to measurements made in D_2O unless stated otherwise. [c] Measured in MeCN.

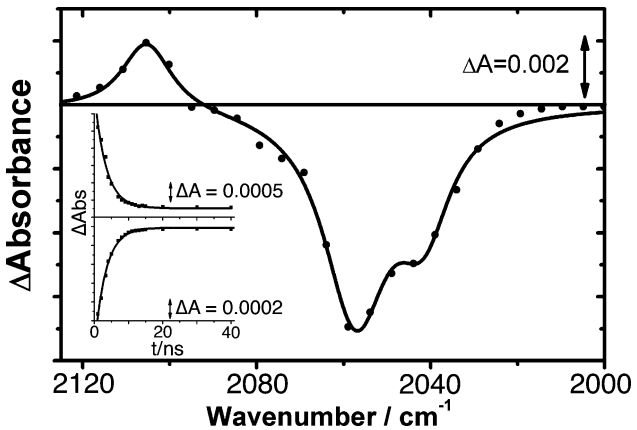

Fig. 13 IR difference spectrum of $K_2[Ru(bpym)(CN_4)]$ in D_2O obtained 100 ps after 400 nm excitation into the ^{1}MLCT absorption manifold. Inset are kinetic traces showing decay of the transient (top) and recovery of the bleach (below) from which excited-state lifetimes were derived.

weakness of the transient ν(CN) vibration compared to the ground state vibration is consistent with our previous observations[12b] and suggests that the dipole of the C–N bonds is reduced in the ^{3}MLCT excited state. This is reasonable, as cyanide ligands formally have the negative charge on the C atom: transient oxidation of Ru(II) to Ru(III) will reduce the partial negative charge on the coordinated C atom and hence diminish the C–N dipoles, leading to weaker IR absorptions. The inherent weakness of the transient ν(CN) signals is exacerbated by the fact that the transient signal at $\approx$ 2100 cm^{-1} will be partially overlapping with the bleach of the weak, highest-energy ν(CN) vibration in the ground state which will reduce the apparent intensity of the transient peak still further. A consequence of this is that only the most intense ν(CN) transient peak can clearly be seen in the difference spectra.

Analogous behaviour is shown by all of the complexes in D_2O, with a shift to higher energy of the most intense ν(CN) vibration of between 46 and 52 cm^{-1} in the ^{3}MLCT excited state, as shown by a bleach of the ground-state vibrations and appearance of a much weaker transient peak at higher energy (Table 2). These values are the same within the limits of accuracy of the experiment, given a combination of 4 cm^{-1} resolution for the spectra and the low intensity of the transients. The fast timescale of this technique allowed us to determine accurately the lifetime of **Ru-bpym**, which could not be determined by luminescence methods as the luminescence was too weak and short-lived. Fig. 13 shows the IR difference spectrum for this complex and the kinetics of transient decays and parent recovery. The rates derived from these data match closely and give $\tau = 3.4$ ns for the ^{3}MLCT excited state in D_2O.

Two of the complexes were sufficiently soluble in MeCN to allow study of the effect of changing solvent on their transient IR behaviour. **Ru-dmb** and **Ru-bpym** showed similar difference spectra shortly (picoseconds) after excitation to those seen in water, with the exception that the shift to higher energy of the main ν(CN) vibration was less, being 36 cm^{-1} for **Ru-dmb** (*cf.* 46 cm^{-1} in D_2O) and 30 cm^{-1} for **Ru-bpym** (*cf.* 48 cm^{-1} in D_2O). This appears to be principally a consequence of the fact that the most intense ν(CN) vibration in the ground state is at higher energy in MeCN than in water [for **Ru-dmb**, 2068 *vs.* 2049 cm^{-1}; for **Ru-bpym**, 2068 *vs.* 2057 cm^{-1}], an effect which must arise from differences in hydrogen-bonding with the solvent. By observing transient IR spectra at a range of delays after excitation we measured the lifetime of the ^{3}MLCT excited state of **Ru-bpym** in MeCN to be 250 ps, an order of magnitude shorter than the value observed in water, in keeping with the general trend expected for complexes of this series.[1] Similarly, the ^{3}MLCT lifetime of **Ru-PBE** plummeted from 471 ns (measured by luminescence) to 4.5 ns (measured from decay of the transients in the excited-state IR spectrum) on changing the solvent from D_2O to dmf (Table 1).

Conclusions

It is clear that this small family of new analogues of $[Ru(bpy)(CN)_4]^{2-}$ is of interest for a range of distinct reasons. The combination of their ability to form coordination networks in the solid state, their solvent-dependent photophysical properties, and the presence of the IR-active cyanide groups to monitor excited-state processes, makes this family of complexes exceptionally valuable for both the preparation and the spectroscopic characterisation of polynuclear photophysically-active assemblies.

Experimental

General details

The following compounds were prepared using previously described methods: 3-(2-pyridyl)pyrazole,[19] 1-ethyl-2-(2-pyridyl)-benzimidazole,[20] $K_2[Ru(bpy)(CN)_4]$ (**Ru-bpy**)[1] and $K_2[Ru(phen)(CN)_4]$ (**Ru-phen**).[13] Other organic ligands were purchased from Aldrich and used as received. Potassium hexacyanoruthenate trihydrate was provided on loan by Johnson Matthey plc. ^{1}H NMR spectra were recorded on a Bruker AC 250 or Bruker AMX2

400 spectrometer, and all mass spectra (FAB and EI) on a VG AutoSpec magnetic sector instrument. IR spectra were recorded on a Perkin-Elmer Spectrum One instrument, and UV/Vis spectra on a Cary-50 spectrometer. Cyclic voltammetric measurements were performed with an Ecochimie Autolab-100 potentiostat using a conventional three-electrode configuration (Pt working and auxiliary electrodes, Ag/AgCl reference electrode); the solvent was distilled water containing 0.1 M KCl as base electrolyte. Using this system the redox potential of the $[Fe(CN)_6]^{3-/4-}$ couple was +0.27 V.

Preparations

K_2[Ru(bpym)(CN)$_4$] (Ru-bpym). 2,2′-Bipyrimidine (0.16 g, 1 mmol) and $K_4[Ru(CN)_6]\cdot 3H_2O$ (0.42 g, 0.9 mmol) were added to a solution of distilled water (30 cm^3) acidified with a few drops of HCl (pH = 1.3). The resulting light yellow solution was heated to reflux with stirring for 24 h and then cooled to room temperature. The resulting dark red-brown solution was neutralised with KOH and the solution was evaporated to dryness. The solid residue was dissolved in the minimum quantity of water, and MeOH was added to precipitate unreacted $K_4[Ru(CN)_6]\cdot 3H_2O$ which was filtered off. The residue was again evaporated to dryness, dissolved in the minimum quantity of water; addition of acetone precipitated the complex which was filtered off and washed with acetone. The product was purified by column chromatography on SEPHADEX QAE-25, eluting with aqueous KI (0.15 M). The fraction containing the light orange product was colleted and reduced in volume to 5 cm^3. The complex was precipitated by the addition of acetone and further recrystallized from H_2O/acetone and dried *in vacuo* to give an orange solid that is soluble in water, slightly soluble in MeOH and insoluble in other common organic solvents. Yield: 76%. X-Ray quality crystals were grown by slow evaporation of an aqueous solution of the complex. ^{1}H NMR (D_2O): δ (ppm) 9.45 (2H, dd; bpym $H^{6,6'}$), 9.05 (2H, dd; bpym $H^{4,4'}$), 7.75 (2H, t; bpym $H^{5,5'}$). MS (MALDI-TOF): *m*/*z* 365 $\{HRu(bpym)(CN)_4\}^-$, 338 $\{Ru(bpym)(CN)_3\}^-$. Found: C, 30.4; H, 2.1; N, 23.2%. $K_2[Ru(bpym)(CN)_4]\cdot 2H_2O$ requires C, 30.2; H, 2.1; N, 23.5%.

K_2[Ru(Me$_2$bpy)(CN)$_4$] (Ru-dmb). A solution of 5,5′-dimethyl-2,2′-bipyridine (120 mg, 0.65 mmol) and $K_4[Ru(CN)_6]\cdot 3H_2O$ (320 mg, 0.69 mmol) in aqueous MeOH (1 : 1, 50 cm^3), acidified to pH 3.5 with a few drops of H_2SO_4, was stirred and heated to reflux under N_2 for 48 h. The resulting deep yellow solution was cooled and neutralised with K_2CO_3. The solution was evaporated to dryness, redissolved in the minimum quantity of water, and MeOH was added to precipitate unreacted $K_4[RuCN_6]\cdot 3H_2O$ which was filtered off. The yellow filtrate was again evaporated to dryness and the solid was recrystallised from water/acetone to give $K_2[Ru(Me_2bpy)(CN)_4]$ in 58% yield; its appearance varies between deep red and bright yellow depending on how dry it is. ^{1}H NMR (D_2O): δ (ppm) 8.97 (2H, s; pyridyl $H^6/H^{6'}$), 7.93 (2H, d; pyridyl $H^3/H^{3'}$ or $H^4/H^{4'}$), 7.62 (2H, d; pyridyl $H^4/H^{4'}$ or $H^3/H^{3'}$). ES MS (negative ion mode): *m*/*z* 391 $\{Ru(Me_2bpy)(CN)_4H\}^-$. Found: C, 36.3; H, 3.6; N, 16.2%. $K_2[Ru(Me_2bpy)(CN)_4]\cdot 3H_2O$ requires C, 36.8; H, 3.5; N, 16.1%.

K_2[Ru(pypz)(CN)$_4$] (Ru-pypz). This was made in an identical manner to the preparation of **Ru-dmb** above, using 3-(2-pyridyl)pyrazole as the diimine ligand; the reaction mixture was refluxed for 3 days before cooling and workup. The product was isolated in 61% yield as a green powder. ^{1}H NMR (D_2O): δ (ppm) 9.04 (1H, d; pyridyl H^6), 7.87 (2H, m; pyridyl H^3 and H^4), 7.81 (1H, d; pyrazolyl), 7.35 (1H, m; pyridyl H^5), 6.96 (1H, d; pyrazolyl). ES MS (negative ion mode): *m*/*z* 352 $\{Ru(pypz)(CN)_4H\}^-$. Found: C, 30.1; H, 2.5; N, 20.5%. $K_2[Ru(pypz)(CN)_4]\cdot 3H_2O$ requires: C, 29.9; H, 2.7; N, 20.3%.

K_2[Ru(PBE)(CN)$_4$] (Ru-PBE). This was made in an identical manner to the preparation of **Ru-dmb** above, using 1-ethyl-2-(2-pyridyl)benzimidazole as the diimine ligand; the product was isolated in 85% yield as dark orange flakes. ^{1}H NMR (D_2O): δ (ppm) 9.23 (1H, dd; pyridyl H^6), 8.44 (1H, d; bn H^3), 7.95 (1H, d; pyridyl H^3), 7.80 (1H, t; pyridyl H^4), 7.36 (3H, m; pyridyl H^5 and bn H^4/H^6), 7.23 (1H, t; bn H^5), 4.19 (2H, br q; CH_2), 1.21 (3H, br t; CH_3) (here 'bn' denotes the benzyl ring of the benzimidazolyl fragment). ES MS (negative ion mode): *m*/*z* 468 $\{KRu(PBE)(CN)_4\}^-$, 429 $\{HRu(PBE)(CN)_4\}^-$. Found: C, 38.3; H, 3.2; N, 16.9%. $K_2[Ru(PBE)(CN)_4]\cdot 3.5H_2O$ requires: C, 38.0; H, 3.5; N, 17.2%.

K_2[Ru(κ^2-terpy)(CN)$_4$] (Ru-terpy). This was made in an identical manner to the preparation of **Ru-dmb** above, using 2,2′:6′,2″-terpyridine as the diimine ligand; the product was isolated in 52% yield as deep red flakes. ^{1}H NMR (D_2O): δ (ppm) 9.12 (1H, dd; terpy $H^{6''}$), 8.50 (1H, d; terpy H^6), 8.16 (1H, dd; terpy $H^{3'}$), 8.11 (1H, d; terpy $H^{3''}$), 7.95 (1H, d; terpy H^3), 7.90 (1H, t; terpy $H^{4'}$), 7.85 (1H, td; terpy H^4), 7.81 (1H, td; terpy $H^{4''}$), 7.46 (2H, m; terpy H^5 and $H^{5'}$), 7.37 (1H, dd; terpy $H^{5''}$). Found: C, 40.0; H, 2.6; N, 16.8%. $K_2[Ru(\kappa^2\text{-terpy})(CN)_4]\cdot 3H_2O$ requires C, 40.0; H, 3.0; N, 17.2%.

KEu[Ru(pypz)(CN)$_4$]·10.5H$_2$O. Solutions of **Ru-pypz** (40 mg, 0.093 mmol) in water (2 cm^3) and $EuCl_3\cdot 6H_2O$ (17 mg, 0.046 mmol) in MeOH (2 cm^3) were mixed in a sample vial; the initially-generated precipitate of KCl was filtered off. Slow evaporation of the residual solution over several weeks afforded green single crystals of $KEu[Ru(pypz)(CN)_4]\cdot 10.5H_2O$ in 26% yield (13 mg). The yield was not optimised as we had found in earlier studies that allowing such solutions to evaporate too near to dryness resulted in a mixture of crystalline materials.[8] Found: C, 26.7; H, 3.3; N, 18.1%. $KEu[Ru(pypz)(CN)_4]\cdot 10.5H_2O$ requires: C, 26.7; H, 2.9; N, 18.1%.

KEr[Ru(PBE)(CN)$_4$]$_2$·10H$_2$O. Solutions of **Ru-PBE** (40 mg, 0.072 mmol) in water (2 cm^3) and $ErCl_3\cdot 6H_2O$ (13.7 mg, 0.036 mmol) in MeOH (2 cm^3) were mixed in a sample vial; the initially-generated precipitate of KCl was filtered off. Slow evaporation of the residual solution over several weeks afforded orange single crystals of $KEr[Ru(PBE)(CN)_4]_2\cdot 10H_2O$ in 22% yield (10 mg). The yield was not optimised as we had found in earlier studies that allowing such solutions to evaporate too near to dryness resulted in a mixture of crystalline materials.[8] Found: C, 36.5; H, 3.4; N, 16.3%. $KEr[Ru(PBE)(CN)_4]_2\cdot 7H_2O$ requires: C, 36.4; H, 3.4; N, 16.5%. The crystals lost solvent rapidly after removal from the mother liquor as is clear from the elemental analysis ($\approx$ 7 H_2O present in the isolated crystals after drying compared to 10 in the crystal structure).

Table 3 Bond distances to the K^+ ions in $K_2[Ru(phen)(CN)_4]\cdot 4H_2O$[a,b]

K(2)–O(103)	2.716(8)	K(3)–N(6C)	2.775(11)
K(2)–O(103B)	2.751 (8)	K(3)–N(6B)	2.788(13)
K(2)–N(5A)	2.791(11)	K(3)–N(3)	3.017(14)
K(2)–N(5)	2.908(13)	K(3)–N(5)	3.029(12)
K(2)–N(6B)	2.983(13)	K(3)–C(13)	3.077(14)
K(2)–N(2B)	3.005(13)	K(3)–C(15)	3.133(15)
K(2)–C(16B)	3.046(16)	K(3)–O(100)	3.229(7)
K(2)–C(14B)	3.073(14)	K(3)–O(101B)	3.025(9)
K(2)···K(3A)	4.367(6)	K(3)–O(101)	2.714(8)
K(2)···K(2A)	3.968(4)	K(3)···K(3A)	3.923(4)

[a] The bond lengths and angles around the Ru(II) centre unit are unremarkable [Ru–C, 1.98–2.06 Å; Ru–N, 2.10–2.11 Å]. [b] Symmetry operations for generating equivalent atoms: A: $x, -y+1, z-1/2$. B: $x, -y+1, z+1/2$. C: $x, y, z+1$.

Table 4 Bond distances to the K^+ ions in $K_2[Ru(bpym)(CN)_4]\cdot 3H_2O$[a,b]

K(2)–O(3)	2.673(2)	K(2)–O(1E)	2.914(2)
K(2)–O(2)	2.741(2)	K(2)–N(2)	2.919(2)
K(2)–N(8C)	2.776(3)	K(2)–N(3)	2.941(2)
K(2)–N(7D)	2.880(2)		
K(1)–O(1)	3.235(2)	K(1)–C(12)	3.214(3)
K(1)–O(3A)	2.727(2)	K(1)–N(8)	3.320(3)
K(1)–O(2A)	2.910(2)	K(1)–C(9B)	3.418(3)
K(1)–C(11B)	3.232(3)	K(1)–N(5B)	3.277(2)
K(1)–N(7B)	2.938(3)	K(1)–C(11)	3.284(3)
K(1)–C(10)	3.116(3)	K(1)–N(7)	3.443(3)
K(1)–N(6)	3.133(3)		
K(2)···K(1D)	4.0473(9)	K(2)···K(1C)	4.2049(9)

[a] The bond lengths and angles around the Ru(II) centre unit are unremarkable [Ru–C, 1.98–2.05 Å; Ru–N, 2.11 Å]. [b] Symmetry operations for generating equivalent atoms: A: $-x+1, y-1/2, -z+3/2$. B: $x, -y+3/2, z+1/2$. C: $-x+1, -y+2, -z+2$. D: $-x+1, y+1/2, -z+3/2$. E: $-x+2, -y+2, -z+2$.

Table 5 Bond distances in $[Ru(\kappa^2\text{-terpy})(CN)_4]\cdot MeOH\cdot 0.5H_2O$[a]

Ru(1)–C(1)	1.970(7)	Ru(1)–C(3)	2.057(7)
Ru(1)–C(4)	1.977(6)	Ru(1)–N(11)	2.105(5)
Ru(1)–C(2)	2.045(7)	Ru(1)–N(21)	2.190(5)
K(1)–N(1A)	2.681(6)	K(1)–N(2C)	2.895(5)
K(1)–N(4B)	2.769(5)	K(1)–O(101C)	3.176(8)
K(1)–N(2)	2.827(6)	K(1)–O(101)	3.395(8)
K(2)–N(4)	2.866(6)	K(2)–C(1B)	3.086(6)
K(2)–N(31D)	2.881(6)	K(2)–C(4)	3.134(6)
K(2)–N(4B)	2.908(6)	K(2)–N(2)	3.144(5)
K(2)–N(1B)	2.943(6)	K(2)–C(4B)	3.168(6)
K(2)–O(101)	2.948(7)	K(2)–C(2)	3.330(6)
K(1)···K(2)	4.238(2)	K(1)···K(2C)	4.934(2)
K(1)···K(2B)	4.254(2)	K(1)···K(1C)	3.454(3)

[a] Symmetry operations for generating equivalent atoms: A: $x, y+1, z$. B: $-x, y+1/2, -z+1/2$. C: $-x+1/2, -y+3/2, -z+1/2$. D: $-x, y-1/2, -z+1/2$.

Table 6 Bond distances in $KEr[Ru(PBE)(CN)_4]_2\cdot 10H_2O$[a,b]

Ru(2)–C(13)	1.94(2)	Ru(2)–C(7)	1.964(17)
Ru(2)–C(10)	1.93(2)	Ru(2)–N(2)	2.104(12)
Ru(2)–C(14)	1.95(2)	Ru(2)–N(8)	2.129(14)
Er(1)–N(4)	2.365(12)	Er(1)–O(3)[c]	2.44(3)
Er(1)–N(6A)	2.370(18)	Er(1)–O(7)[c]	2.51(3)
Er(1)–O(1)	2.374(12)		

[a] Bond distances around K^+ are not quoted due to extensive disorder involving both the K+ ions themselves and some of the coordinated water ligands. [b] Symmetry operations for generating equivalent atoms (A): $-x, 1-y, -z$. [c] 50% site occupancy.

$[Eu(NO_3)(H_2O)_5][Ru(bpym)(CN)_4]$. Solutions of **Ru-bpym** (0.020 g, 40 μmol) in water (1 cm^3) and $Eu(NO_3)_3\cdot 6H_2O$ (0.086 g, 0.25 mmol) in water (2 cm^3) were mixed to give a deep orange solution which was stirred for 10 min. Slow evaporation of the solution afforded orange platelike crystals suitable for X-ray diffraction which were filtered off and washed with methanol. Yield: 77%. Found: C, 21.4; H, 2.1; N, 18.5%. Required for $[Eu(NO_3)(H_2O)_5][Ru(bpym)(CN)_4]$: C, 21.6; H, 2.4; N, 18.9%.

Luminescence measurements

Emission measurements were performed on an Edinburgh Instruments FLS920 combined fluorescence lifetime and steady state spectrometer. The optical density was adjusted to *ca.* 0.2–0.5 at the excitation wavelength. Steady state emission and excitation spectra were obtained with a xenon arc lamp as the excitation source and were corrected for detector sensitivity. Lifetimes were determined using the time-correlated single photon counting method with a

Table 7 Bond distances in $KEu[Ru(pypz)(CN)_4]\cdot 10.5H_2O$[a]

Eu(1)–O(4)	2.363(4)	Eu(2)–O(10)	2.351(4)
Eu(1)–O(1)	2.382(4)	Eu(2)–O(9)	2.359(4)
Eu(1)–O(3)	2.431(4)	Eu(2)–O(7)	2.390(4)
Eu(1)–O(2)	2.432(4)	Eu(2)–O(6)	2.473(4)
Eu(1)–O(5)	2.448(4)	Eu(2)–O(8)	2.495(4)
Eu(1)–N(7)	2.467(5)	Eu(2)–N(14)	2.496(4)
Eu(1)–N(21)	2.507(4)	Eu(2)–N(20)	2.498(4)
Eu(1)–N(13A)	2.511(4)	Eu(2)–N(27)	2.499(4)
Ru(1)–C(11)	1.966(5)	Ru(3)–C(35)	1.969(5)
Ru(1)–C(12)	1.977(5)	Ru(3)–C(36)	1.980(5)
Ru(1)–C(10)	2.034(5)	Ru(3)–C(34)	2.036(5)
Ru(1)–C(9)	2.035(5)	Ru(3)–C(33)	2.043(5)
Ru(1)–N(3)	2.112(4)	Ru(3)–N(17)	2.107(4)
Ru(1)–N(1)	2.146(4)	Ru(3)–N(15)	2.150(4)
Ru(2)–C(23)	1.973(5)	Ru(4)–C(48)	1.968(5)
Ru(2)–C(24)	1.974(5)	Ru(4)–C(47)	1.981(5)
Ru(2)–C(22)	2.019(5)	Ru(4)–C(45)	2.022(5)
Ru(2)–C(21)	2.038(5)	Ru(4)–C(46)	2.033(5)
Ru(2)–N(10)	2.114(4)	Ru(4)–N(24)	2.115(4)
Ru(2)–N(8)	2.149(4)	Ru(4)–N(22)	2.145(4)
K(1)–N(28C)	2.827(5)	K(2)–N(6)	2.986(5)
K(1)–N(4D)	2.981(5)	K(2)–N(19)	3.408(5)
K(1)–N(6D)	3.107(5)	K(2)–N(21)	3.371(4)
K(1)–N(11)	3.141(5)	K(2)–N(26B)	3.155(5)
K(1)–N(13)	3.025(5)	K(2)–N(27B)	3.263(5)
K(1)–C(23)	3.193(5)	K(2)–C(48B)	3.318(5)
K(1)–C(9D)	3.276(5)	K(2)–C(46B)	3.322(5)
K(1)–C(21)	3.327(5)	K(2)–C(11)	3.372(5)
K(1)–C(11D)	3.329(5)	K(2)–O(12)	2.808(5)
K(1)–O(11)	2.733(5)	K(2)–O(13)	2.730(5)

[a] Symmetry operations for generating equivalent atoms: A $1-x, 1-y, 1-z$. B $1-x, 1-y, -z$. C $1-x, -y, -z$. D $x, -1+y, z$.

Table 8 Bond distances in $[Eu(NO_3)(H_2O)_5][Ru(bpym)(CN)_4]$[a]

Ru(1)–C(11)	1.968(4)	Ru(1)–C(13)	2.052(4)
Ru(1)–C(12)	1.982(4)	Ru(1)–N(1)	2.116(3)
Ru(1)–C(10)	2.037(4)	Ru(1)–N(3)	2.117(3)
Eu(2)–O(2)	2.375(3)	Eu(2)–O(5)	2.479(3)
Eu(2)–O(8)	2.407(3)	Eu(2)–N(7A)	2.494(3)
Eu(2)–O(1)	2.438(3)	Eu(2)–O(3)	2.577(3)
Eu(2)–O(4)	2.444(2)	Eu(2)–O(6)	2.774(3)
Eu(2)–N(6)	2.449(3)		

[a] Symmetry transformations used to generate equivalent atoms: A: $1-x, 2-y, 1/2+z$.

Table 9 Crystallographic data for the six crystal structures[a]

Complex	K_2[Ru(phen)-$(CN)_4$]·$4H_2O$	K_2[Ru(bpym)-$(CN)_4$]·$3H_2O$	[Ru(κ²-terpy)$(CN)_4$]·MeOH·$0.5H_2O$	KEr[Ru(PBE)-$(CN)_4]_2$·$10H_2O$	KEu[Ru(pypz)-$(CN)_4]_2$·$10.5H_2O$	[$Eu(NO_3)(H_2O)_5$][Ru(bpym)$(CN)_4$]
Formula	$C_{16}H_{16}K_2N_6O_4Ru$	$C_{12}H_{12}K_2N_8O_3Ru$	$C_{20}H_{16}K_2N_7O_{1.5}Ru$	$C_{36}H_{46}ErKN_{15}O_9Ru_2$	$C_{48}H_{70}Eu_2K_2N_{28}O_{21}Ru_4$	$C_{12}H_{16}EuN_9O_8Ru$
M	535.62	495.57	557.67	1241.38	2161.72	667.37
T/K	150	150	173	173	150	150
Crystal system, space group	Monoclinic, Cc[b]	Monoclinic, $P2_1/c$	Monoclinic, $I2/a$	Monoclinic, $C2/c$	Triclinic, $P\bar{1}$	Orthorhombic, $Pna2_1$
a/Å	10.2914(16)	6.5658(7)	17.648(3)	28.636(6)	14.0042(16)	24.791(2)
b/Å	30.116(5)	23.435(2)	8.9779(16)	14.487(3)	16.3639(19)	6.5425(6)
c/Å	6.6628(11)	11.7021(12)	29.053(6)	15.487(3)	18.520(2)	12.4486(12)
α/°	90	90	90	90	113.599(2)	90
β/°	101.862(3)	93.836(2)	105.468(3)	103.05(3)	103.578(2)	90
γ/°	90	90	90	90	91.274(2)	90
V/Å^3	2020.9(6)	1796.6(3)	4436.5(14)	6259(2)	3748.2(7)	2019.1(3)
Z	4	4	8	4	2	4
D_{calc}/Mg m^{-3}	1.760	1.832	1.670	1.317	1.915	2.195
μ/mm^{-1}	1.224	1.367	1.112	1.921	2.630	3.888
Reflections collected	11781	19966	14915	30015	42204	21936
Independent reflections	4359 (R_{int} = 0.0847)	4104 (R_{int} = 0.0587)	4950 (R_{int} = 0.0650)	5504 (R_{int} = 0.1580)	16650 (R_{int} = 0.0360)	4622 (R_{int} = 0.0299)
Data/restraints/parameters	4359/63/262	4104/0/235	4950/0/285	5504/0/331	16650/0/946	4622/1/281
Final $R1$, $wR2$ indices[c]	0.0548, 0.1191	0.0297, 0.0671	0.0586, 0.1476	0.0915, 0.3235	0.0396, 0.0952	0.0185, 0.0425
Largest diff. peak and hole/ e Å^{-3}	1.021, −0.983	0.636, −0.617	1.167, −0.916	1.877, −1.897	2.191, −0.967	0.808, −0.411

[a] All measurements made on a Bruker SMART diffractometer using Mo-Kα radiation. [b] PLATON suggests that $C2/c$ is also possible but this results in a poorer refinement. The Flack parameter of 0.29(8) for this structure reflects the presence of racemic twinning. [c] $R1$ value is based on selected data [with $I > 2\sigma(I)$]; $wR2$ value is based on all data.

hydrogen lamp as the excitation source. Emission quantum yields, Φ_{em}, were determined using a solution of $[Ru(bpy)_3]Cl_2$ in D_2O as the emission standard.

Time-resolved infrared spectroscopy

TRIR experiments were carried out using the PIRATE apparatus at the Central Laser Facility of the CCLRC Rutherford Appleton Laboratory. This apparatus has been described in detail previously.[30] Part of the output from a 1 kHz, 800 nm, 150 fs, 2 mJ Ti-sapphire oscillator/regenerative amplifier (Spectra Physics Tsunami/Spitfire) was used to pump a white light continuum seeded β-BaB_2O_4 (BBO) optical parametric amplifier (OPA). The signal and idler produced by this OPA were difference frequency mixed in a type I $AgGaS_2$ crystal to generate tuneable mid-infrared pulses (*ca.* 150 cm^{-1} FWHM, 1 μJ), which were split to give probe and reference pulses. Second harmonic generation of the residual 800 nm light provided 400 nm pump pulses. Both the pump and probe pulses were focused to a diameter of 200–300 μm in the sample. Changes in infrared absorption at various pump–probe time delays were recorded by normalising the outputs from a pair of 64-element MCT infrared linear array detectors on a shot-by-shot basis.

X-Ray crystallography

X-Ray crystallographic data are summarised in Tables 3–9. For each compound a suitable crystal was coated with hydrocarbon oil and attached to the tip of a glass fibre and transferred to Bruker-SMART diffractometer with an Oxford Cryosystems low temperature system. Data were collected using graphite-monochromated Mo-Kα radiation, λ = 0.71073 Å. The data were corrected for Lorentz and polarisation effects. Absorption corrections were applied in each case using SADABS,[31] and structure solution and refinement was carried out using SHELXS-97 and SHELXL-97 respectively.[32,33] The structures were solved by direct methods or heavy atom Patterson methods and refined by full matrix least squares methods on F^2. Hydrogen atoms were placed geometrically and refined with a riding model and with U_{iso} constrained to be 1.2 (1.5 for methyl groups) times U_{eq} of the carrier atom. All non-hydrogen atoms were refined anisotropically. The only structural determination that presented any problems was $KEr[Ru(PBE)(CN)_4]_2 \cdot 10H_2O$, for which the crystals were thin and poorly-diffracting plates and which also suffered from extensive disorder. The K^+ ion K(1), which lies in a general position, has only 50% site occupancy such that it is effectively disordered above and below the diamondoid Ru–CN–Er chain; this is shown in more detail in Fig. 8. Accordingly the water molecules coordinated to K(1) [O(3), O(4), O(7)], and some of the lattice water molecules [O(2), O(5), O(6), O(8), O(9)] likewise have only 50% site occupancy. The final $R1$ value of 9.15% reflects these problems but the gross structure of the diamondoid chain is perfectly clear.

CCDC reference numbers 276244–276249.

See http://dx.doi.org/10.1039/b509042c for crystallographic data in CIF or other electronic format.

Acknowledgements

We thank the EPSRC for studentships to W. Z. A., T. L. E. and H. E. F., and the Spanish Ministry of Science for a post-doctoral

grant (to J.-M. H.). We also thank Johnson Matthey for the loan of some potassium hexacyanoruthenate.

References

1 C. J. Timpson, C. A. Bignozzi, B. P. Sullivan, E. M. Kober and T. J. Meyer, *J. Phys. Chem.*, 1996, **100**, 2915.

2 M. A. Rampi, M. T. Indelli, F. Scandola, F. Pina and A. J. Parola, *Inorg. Chem.*, 1996, **35**, 3355; C. D. Borsarelli, S. E. Braslavsky, M. T. Indelli and F. Scandola, *Chem. Phys. Lett.*, 2000, **317**, 53; N. R. M. Simpson, M. D. Ward, A. Farran Morales, B. Ventura and F. Barigelletti, *J. Chem. Soc., Dalton Trans.*, 2002, 2455; G. Bergamini, C. Saudan, P. Ceroni, M. Maestri, V. Balzani, M. Gorka, S.-K. Lee, J. van Heyst and F. Vögtle, *J. Am. Chem. Soc.*, 2004, **126**, 16466.

3 C. A. Bignozzi, C. Chiorboli, M. T. Indelli, M. A. R. Scandola, G. Varani and F. Scandola, *J. Am. Chem. Soc.*, 1986, **108**, 7872.

4 A. Juris, V. Balzani, F. Barigeletti, S. Campagna, P. Belser and A. von Zelewsky, *Coord. Chem. Rev.*, 1988, **84**, 85; V. Balzani, A. Juris, M. Venturi, S. Campagna and S. Serroni, *Chem. Rev.*, 1996, **96**, 759; C. A. Bignozzi, J. N. Schoonover and F. Scandola, *Prog. Inorg. Chem.*, 1997, **44**, 1; M. D. Ward, *Chem. Soc. Rev.*, 1997, **26**, 365.

5 J. K. Evku and K. R. Mann, *Chem. Mater.*, 1999, **11**, 1425.

6 N. R. M. Simpson, M. D. Ward, A. Farran Morales and F. Barigelletti, *J. Chem. Soc., Dalton Trans.*, 2002, 2449.

7 M. T. Indelli, M. Ghirotti, A. Prodi, C. Chiorboli, F. Scandola, N. D. McClenaghan, F. Puntoriero and S. Campagna, *Inorg. Chem.*, 2003, **42**, 5489.

8 T. A. Miller, J. C. Jeffery, M. D. Ward, H. Adams, S. J. A. Pope and S. Faulkner, *Dalton Trans.*, 2004, 1524; G. M. Davies, S. J. A. Pope, H. Adams, S. Faulkner and M. D. Ward, *Inorg. Chem.*, 2005, **44**, 4656.

9 T. A. Miller, J. C. Jeffery and M. D. Ward, *CrystEngComm*, 2003, **5**, 495.

10 C. A. Bignozzi, C. Chiorboli, M. T. Indelli, F. Scandola, V. Bertolasi and G. Gilli, *J. Chem. Soc., Dalton Trans.*, 1994, 2391.

11 J. Dyer, W. J. Blau, C. G. Coates, C. M. Creely, J. D. Gavey, M. W. George, D. C. Grills, S. Hudson, J. M. Kelly, P. Matousek, J. J. McGarvey, J. McMaster, A. W. Parker, M. Towrie and J. A. Weinstein, *Photochem. Photobiol. Sci.*, 2003, **2**, 542; M. W. George, F. P. A. Johnson, J. R. Westwell, P. M. Hodges and J. J. Turner, *J. Chem. Soc., Dalton Trans.*, 1993, 2977.

12 (*a*) M. K. Kuimova, M. Y. Mel'nikov, J. A. Weinstein and M. W. George, *J. Chem. Soc., Dalton Trans.*, 2002, 2857; (*b*) S. Encinas, A. F. Morales, F. Barigelletti, A. M. Barthram, C. M. White, S. M. Couchman, J. C. Jeffery, M. D. Ward, D. C. Grills and M. W. George, *J. Chem. Soc., Dalton Trans.*, 2001, 3312.

13 M. Kovács and A. Horváth, *Inorg. Chim. Acta*, 2002, **335**, 69.

14 M. Ohba and H. Okawa, *Coord. Chem. Rev.*, 2000, **198**, 313; M. Verdaguer, A. Bleuzen, V. Marvaud, J. Vaissermann, M. Seuleiman, C. Desplanches, A. Scuiller, C. Train, R. Garde, G. Gelly, C. Lomenech, I. Rosenman, P. Veillet, C. Cartier and F. Villain, *Coord. Chem. Rev.*, 1999, **190–192**, 1023; K. R. Dunbar and R. A. Heintz, *Prog. Inorg. Chem.*, 1997, **45**, 283.

15 T. Korzeniak, K. Stadnicka, M. Rams and B. Sieklucka, *Inorg. Chem.*, 2004, **43**, 4811; J.-M. Herrera, A. Bleuzen, Y. Dromzee, M. Julve, F. Lloret and M. Verdaguer, *Inorg. Chem.*, 2003, **42**, 7052; Z. J. Zhong, H. Seino, Y. Mizobe, M. Hidai, M. Verdaguer, S. Ohkoshi and K. Hashimoto, *Inorg. Chem.*, 2000, **39**, 5095; T. Kashiwagi, S. Ohkoshi, H. Seino, Y. Mizobe and K. Hashimoto, *J. Am. Chem. Soc.*, 2004, **126**, 5024.

16 L. M. Toma, F. S. Delgado, C. Ruiz-Pérez, R. Carrasco, J. Cano, F. Lloret and M. Julve, *Dalton Trans.*, 2004, 2836.

17 C. E. Plecnik, S. Liu and S. G. Shore, *Acc. Chem. Res.*, 2003, **36**, 499.

18 M. A. Rawashdeh-Omary, C. L. Larochelle and H. H. Patterson, *Inorg. Chem.*, 2000, **39**, 4527.

19 P. L. Jones, A. J. Amoroso, J. C. Jeffery, J. A. McCleverty, E. Psillakis, L. H. Rees and M. D. Ward, *Inorg. Chem.*, 1997, **36**, 10.

20 L. Huang, K. Z. Wang, C. H. Huang, F. Y. Li and Y. Y. Huang, *J. Mater. Chem.*, 2001, **11**, 790.

21 M. T. Indelli, C. A. Bignozzi, F. Scandola and J.-P. Collin, *Inorg. Chem.*, 1998, **37**, 6084.

22 R. Chotalia, E. C. Constable, M. J. Hannon and D. A. Tocher, *J. Chem. Soc., Dalton Trans.*, 1995, 3571.

23 (*a*) S. M. Contakes and T. B. Rauchfuss, *Chem. Commun.*, 2001, 553; (*b*) S. M. Contakes and T. B. Rauchfuss, *Angew. Chem., Int. Ed.*, 2000, **39**, 1984; (*c*) M. L. Kuhlman and T. B. Rauchfuss, *J. Am. Chem. Soc.*, 2003, **125**, 10084.

24 (*a*) J. X. Hu, L. J. Barbour and G. W. Gokel, *Collect. Czech. Chem. Commun.*, 2004, **69**, 1050; (*b*) J. Hu and G. W. Gokel, *Chem. Commun.*, 2003, 2537; (*c*) G. W. Gokel, *Chem. Commun.*, 2003, 2847; (*d*) J. Hu, L. J. Barbour and G. W. Gokel, *J. Am. Chem. Soc.*, 2001, **123**, 9486.

25 (*a*) R. H. Fabian, D. M. Klassen and R. W. Sonntag, *Inorg. Chem.*, 1980, **19**, 1977; (*b*) J. M. Kelly, C. Long, C. M. O'Connell, J. G. Vos and A. H. A. Tinnemans, *Inorg. Chem.*, 1983, **22**, 2818; (*c*) E. C. Constable, M. J. Hannon, A. M. W. Cargill Thompson, D. A. Tocher and J. V. Walker, *Supramol. Chem.*, 1993, **2**, 243; (*d*) A. M. Barthram, M. D. Ward, A. Gessi, N. Armaroli, L. Flamigni and F. Barigelletti, *New J. Chem.*, 1998, **22**, 913; (*e*) D. A. Bardwell, F. Barigelletti, R. L. Cleary, L. Flamigni, M. Guardigli, J. C. Jeffery and M. D. Ward, *Inorg. Chem.*, 1995, **33**, 2438.

26 (*a*) T. J. Meyer, *Pure Appl. Chem.*, 1986, **58**, 1193; (*b*) A. Juris, V. Balzani, F. Barigelletti, S. Campagna, P. Belser and A. von Zelewsky, *Coord. Chem. Rev.*, 1988, **84**, 85; (*c*) K. Kalyanasundaram, *Coord. Chem. Rev.*, 1982, **46**, 159.

27 L. A. Worl, R. Duesing, P. Chen, L. Della Ciana and T. J. Meyer, *J. Chem. Soc., Dalton Trans.*, 1991, 849.

28 N. M. Shavaleev, G. Accorsi, D. Virgili, Z. R. Bell, T. Lazarides, G. Calogero, N. Armaroli and M. D. Ward, *Inorg. Chem.*, 2005, **44**, 61.

29 (*a*) E. C. Whittle, J. A. Weinstein, M. W. George and K. S. Schanze, *Inorg. Chem.*, 2001, **40**, 4053; (*b*) M. Hissler, M. Connick, D. K. Geiger, J. E. McGarrah, D. Lipa, R. J. Lachiotte and R. Eisenberg, *Inorg. Chem.*, 2000, **39**, 447.

30 (*a*) M. Towrie, D. C. Grills, J. Dyer, J. A. Weinstein, P. Matousek, R. Barton, P. D. Bailey, N. Subramaniam, W. M. Kwok, C. S. Ma, D. Phillips, A. W. Parker and M. W. George, *Appl. Spectrosc.*, 2003, **57**, 367; (*b*) M. Towrie, A. Gabrielsson, P. Matousek, A. W. Parker, A. M. B. Rodriguez and A. Vlcek, *Appl. Spectrosc.*, 2005, **59**, 467.

31 G. M. Sheldrick, *SADABS, A program for absorption correction with the Siemens SMART area-detector system*, University of Göttingen, Germany, 1996.

32 G. M. Sheldrick, *SHELXS-97, a Program for Automatic Solution of Crystal Structures*, University of Göttingen, Germany, 1997.

33 G. M. Sheldrick, *SHELX-97, A Program for crystal structure refinement*, University of Göttingen, Germany, 1997.

